JOURNAL OF CATALYSIS 103, 357–365 (1987)

Selective Oxidation Catalysts Containing Antimony for the Conversion of 1-Butene to Butadiene

I. Preparation and Characterization

G. I. STRAGUZZI,[1] K. B. BISCHOFF, T. A. KOCH, AND G. C. A. SCHUIT

Center for Catalytic Science and Technology, Department of Chemical Engineering, University of Delaware, Newark, Delaware 19716

Received February 9, 1986; revised August 26, 1986

$FeSbO_4$ catalysts containing "excess" surface antimony are active for the selective oxidative dehydrogenation of 1-butene to butadiene. In this paper, the synthesis and characterization of a series of $MSbO_4$, with M = Fe, Al, Cr, and Rh, and $CoSb_2O_6$ catalysts are reported. Synthesis techniques included precipitation from slurry, solid-state reaction, and impregnation. Characterization of the catalysts has been performed using X-ray diffraction, X-ray fluorescence, and X-ray photoelectron spectroscopy. © 1987 Academic Press, Inc.

1. INTRODUCTION

In 1948, propene was first transformed to acrolein using cuprous oxide as the catalyst, with a yield of about 50% (*1*). In 1959, the yield was improved by using a bismuth–molybdate catalyst (*2, 3*). At the same time it was observed that a gaseous mixture of propene, air, and ammonia when passed over this catalyst formed acrylonitrile (*4*). The commercial vapor-phase oxidation and ammoxidation was developed by Standard Oil of Ohio (SOHIO). In 1965, Adams (*5*) found that, with the same catalyst, butadiene could be produced from butene.

A more selective uranium–antimony catalyst for the same set of reactions was introduced in 1965 (*6*). An iron–antimony catalyst was developed to further eliminate the problems of uranium, and is still used in Japan (*7–10*). In 1970, SOHIO introduced multicomponent catalysts (*11*). They are composed of a variety of elements including Ni, Co, Fe, Mn, P, and P, but always contain Bi and Mo.

The independent research done with these catalytic systems has approximately followed their historic development. Most of the studies have focused on bismuth–molybdates and there is now a fairly precise picture of how this catalyst works (*12–14*).

In contrast to bismuth–molybdate, the uranium–antimony catalysts are not as well understood. Although a two-site mechanism seems also to apply, roles of the individual cations are not clear (*15*). Similarly, there is controversy in the literature about the role of each component in the Sn–Sb and Fe–Sb systems, both of which have been extensively studied.

After reviewing models for the catalytic sites, Schuit and Gates (*12*) concluded that in all antimony-containing catalysts, antimony oxide may be considered to be simply an inert component that covers up most of the surface of an active component: UO_3, SnO_2, or Fe_2O_3. The catalytic sites would then be patches exposed under an inert overlayer.

According to this hypothesis, the problem of designing a selective oxidation catalyst would be limited to knowing how to control the size and distribution of such an inert overlayer and how to regulate the amount of oxygen provided by the active phase.

[1] To whom correspondence should be addressed.

0021-9517/87 $3.00

However, the problem of selectivity in mixed oxide goes beyond a geometric patching effect. The objective of this work was to defined the electronic effect on activity and selectivity within a class of mixed oxides catalysts for which the crystallographic structure has been kept constant.

The class was selected to be isostructural and also to have Sb^{5+} as one of the components. By preserving both the structure and the identity of one of the elements, a separation of geometric from electronic effects could be attempted.

The methods used as test reactions are the oxidative dehydrogenation of 1-butene and carbon monoxide oxidation in a series of antimonates of general formula: $MSbO_4$. The series $MSbO_4$ (where M is Fe, Al, Cr, Co, Mn, and Rh) includes a known active and selective catalyst for olefin oxidation: $FeSbO_4$, which was selected for purposes of preliminary experimentation to optimize catalyst preparation and operating reaction conditions.

Most of the antimonates selected for study in the present work have statistical rutile structures like $FeSbO_4$ (*17*). Because of this common structure, the replacement of Fe^{3+} by M in $MSbO_4$ was expected to identify the role of the second metal in changing the electronic factor, relative to antimony.

The surface composition of every antimonate was varied by impregnation. These experiments were directed toward elucidation of effects that are geometric, i.e., connected to changes in the amount of active oxygen. The working hypothesis assumes that the oxygens at the surface can be divided into two groups. One group is bonded to a transition-metal cation and is, in principle, reactive; i.e., these oxygens can interact with olefins or CO. The other type of oxygen is the type observable on oxides such as Sb_2O_5. They are hardly active for catalytic oxidation but can eliminate O_2 to form a lower oxide such as Sb_2O_3. It was also possible to study the chemical effect of changing the transition-metal cation at the surface while preserving the bulk composition and structure. Thus, studies were done on $MSbO_4$ rutile-structure antimonate impregnated with extra antimony, extra M, and extra Fe in the case of M being not only Fe, but also Al and Cr.

The bulk properties of the catalysts were characterized by X-ray diffraction (XRD) and X-ray fluorescence, their surfaces areas were determined by the BET method, and surface composition was characterized by X-ray photoelectron spectroscopy (XPS).

The purpose of this paper is to present detailed aspects of the preparation and characterization of these systems. Their catalytic performance will be described in the second part (*16*).

2. EXPERIMENTAL METHODS

2.A. Catalyst Preparation

2.A.1. Synthesis of pure phases. The $MSbO_4$ catalysts with tetragonal (rutile) structure used in this work may be obtained by precipitation (*18, 19*) or by mixing antimony oxide with M compounds (*20, 21*). An exploratory study was performed with the iron–antimony system to determine which was more effective.

As shown in Table 1, the coprecipitation method gave a single-phase system with higher surface area; which is consistent with Zenkovets (*22*).

Qualitative X-ray fluorescence was used to check the purity of the samples.

The samples were calcined and cooled in flowing air. The temperature was raised at 2°C/min to the desired value and maintained there for several hours to obtain the proper phases and surface area. They were characterized as described in Section 2.B.

2.A.2. Impregnation of pure phases. Solutions were prepared from nitrate salts for Fe, Al, Cr, and Co. For antimony impregnation, a solution was prepared using 3.2 g of tartaric acid in 8 ml of distilled water to dissolve 2 g of Sb_2O_3, and then neutralized with 2 ml of NH_4OH.

TABLE 1

Effect of Preparation Method on Fe–Sb–O

Calcination temperature (°C)	Mechanical mixture		Coprecipitation	
	Phase	Surface area (m^2/g)	Phase	Surface area (m^2/g)
500	Highly amorphous mixed Fe,Sb oxides	62	Amorphous	149
700	Mixed Fe,Sb oxides	23	$FeSbO_4 + Sb_2O_4$	45
750	$FeSbO_4 + Sb_2O_4$	11	$FeSbO_4$	34
900	$FeSbO_4 + Sb_2O_4$	5	—	—

The volume of the impregnating solution added was close to the pore volume of the support. The sample was on dried for 12 h and then calcination was carried out at 50°C below the calcination temperature used for the original catalyst, for the same period of time, under a slow flow of air. Some catalysts were calcined in flowing helium instead of air.

2.B. Characterization

2.B.1. BET surface area. The surface area was determined with a Micromeritics Model 2100D Orr surface-area pore-volume analyzer at liquid nitrogen temperature. For samples with surface area below 10 m^2/g, the measurement was repeated using krypton as the adsorbate. The standard deviation of the fitted data was less than 0.05%.

2.B.2. X-ray diffraction. X-ray diffraction patterns were recorded in a range 2θ = 10° to 80° for powdered samples ground to 325 mesh to increase their peak intensity, using a Philips 3500 automated powder diffractometer with a diffracted beam monochromator, nickel-filtered copper radiation at 45 kV and 40 mA. Silica was used as an internal standard.

To improve the signal-to-noise ratio, increased counting times were used. Thus, per 0.02° step, 1 s was used for qualitative purposes; 5 or 10 s for quantitative analysis of fresh and used samples.

Samples calcined below 700°C gave very broad peaks.

2.B.3. X-ray photoelectron spectroscopy. The XPS data were acquired using a Physical Electronics Model 550 ESCA spectrometer. The system used a Mg anode as the X-ray source ($h\nu$ = 1253.6 eV) and spectra were obtained by signal averaging using a PDP-1104 computer. Survey scans were obtained for all samples to identify the elements present on the surface and then detailed spectra of higher resolution were obtained for the elements of interest. The samples were prepared by grinding to a fine powder and sprinkling on vacuum-compatible adhesive tape. Indium foil was also used as a sample mount in order to check on the validity of the oxygen and carbon concentrations; the adhesive was not found to contribute to those signals since a sufficiently thick and even layer of catalyst had been prepared. Atomic concentrations were obtained using the appropriate sensitivity factors and are accurate to ±10%. Binding energies were referenced to the C (1*s*) peak at 284.6 eV for residual carbon and are accurate to within ±0.2 eV.

The relative area ratio of the Sb $3d_{3/2}$–$3d_{5/2}$ doublet in the 520- to 540-eV region was found to be smaller than the expected 2:3 ratio. The greater-than-expected intensity of the Sb $3d_{5/2}$ line can be explained by a contribution of the oxygen (1*s*) line which appears (*19*) at ca. 531–533

TABLE 2

XRD Data for Iron Antimonate

Catalyst sample	
d(A)	I/I'
3.27	100
2.56	78
2.32	13
2.24	5
1.72	61
1.64	11
1.53	4
1.47	8
1.39	10
1.38	12
1.28	4

eV depending on whether the oxygen is in a bridging or terminal position. A calculated correction was applied to the overlap, using for the theoretical Sb $3d_{5/2}$ = 1.5 Sb $3d_{3/2}$ signal area.

3. EXPERIMENTAL RESULTS

3.A. Iron–Antimony System

3.A.1. $FeSbO_4$. A single phase $FeSbO_4$ was obtained by coprecipitation and calcination in flowing air for 16 h at 750°C. The X-ray diffraction data are listed in Table 2 and show agreement with those of the literature for tetragonal $FeSbO_4$ (*23*). The BET surface area was 34.1 m^2/g.

In Table 3 the surface atomic concentrations of the elements detected by XPS are shown. The data indicate a significant surface enrichment of antimony. The concentration of the Fe and Sb were slightly lower

TABLE 3

XPS Results for Iron Antimonate: Atomic Concentrations (±10%)

	Sb	Fe	C	O
$FeSbO_4$				
Pre-run	20.5	6.3	8.1	65.1
Post-run	19.6	5.9	21.2	53.3

TABLE 4

Effect of Impregnation on XPS Sb/Fe ratio

Catalyst[a]	XPS atomic ratio (Sb 3d/Fe 3p)
5% Sb on A	3.9
4% Sb on B	3.8
1% Sb on A	3.3
A = $FeSbO_4$	3.2
3% Fe on A	3.0
B = $FeSbO_4$ + FeO	2.9
8% Fe on A	2.8

[a] Impregnation given in wt%.

in the used catalyst; however, the Sb/Fe surface ratio did not change. The excess oxygen detected in the fresh catalyst indicates that the carbon was probably present as carbonate. In the used sample, the oxygen to metals (Sb + Fe) ratio is 2.1, indicating that the carbon was probably present as elemental C. There were no observed changes in surface area or bulk structures (XRD).

The iron antimonate was impregnated with different amounts of Sb and Fe. Two different batches of $FeSbO_4$ were used. Batch A, was pure $FeSbO_4$; batch B showed traces of FeO in its XRD pattern, possibly due to a higher calcination temperature (800°C). After impregnation, each catalyst was recalcined at 700°C and characterized before testing for activity and selectivity.

No changes were observed in surface area or bulk structure of either batch after impregnation or after reaction. The effect of the impregnation was shown in the XPS analysis by comparing the ratio of antimony to iron as presented in Table 4.

The XPS showed an increase in carbon for all used samples. The metallic ratio (Sb/Fe) varied within the experimental error; however, there were substantial changes in the shape of the peaks; particularly for the Sb 3d. Wider peaks or a shoulder appeared toward lower binding energies with respect

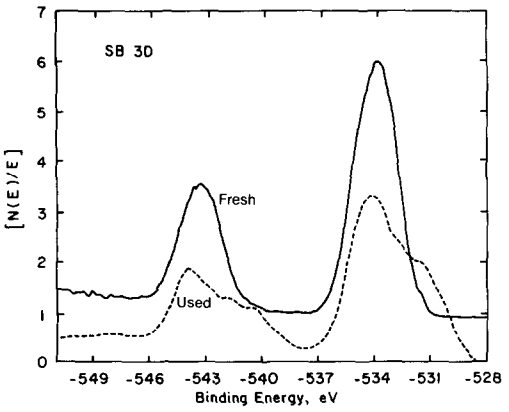

FIG. 1. Qualitative differences of antimony 3*d* bands between fresh and used catalysts.

to the original bands. This feature is shown in Fig. 1 for nonimpregnated $FeSbO_4$.

It is quite difficult to determine the oxidation state of antimony from its 3*d* peak binding energy (*24, 25*). The antimony 3*d* binding energies are greater for the +5 than the +3 oxidation state and are also strongly dependent on the attached ligands and structure. For Sb_2O_4 a separation of only 0.5 eV between the two sets of 3*d* (3/2, 5/2) bands has been reported (*26*).

In stoichiometric rutile $FeSbO_4$, the theoretical oxidation state for Sb is 5+, but there are no restrictions for Sb resulting from impregnation. Fresh samples showed no systematic shifts in binding energies that could be attributed to changes in antimony oxidation state as result of impregnation.

To test the hypothesis of a partial antimony reduction during operation, the following batches of catalysts were prepared and tested.

Batch C. 5 g of iron antimonate precursor was heated in flowing helium during 16 h at 750°C.

Batch D. 5 g of the same coprecipitated precursor was mixed with 2% of Sb_2O_3 and then treated as batch C.

Figure 2 shows the XPS for Sb 3*d* region for batches A, C, and D; all exhibited $FeSbO_4$ rutile structure according to their XRD patterns. Comparison of the spectra for the three samples shows a definite trend to lower oxidation state. The binding energy of the peak at 540.2 eV for oxygen-calcined $FeSbO_4$ coincided with the reported for Sb $3d_{3/2}$ binding energy for Sb_2O_5. Both helium-treated samples exhibited this peak but a lower binding energy shoulder was greatly enhanced. In particular the sample containing extra Sb^{3+} consisted mainly of the lower oxidation state, with only a vestige of the higher oxidation state being present. The Sb/Fe atomic surface ratio for batches C and D were 3.5 and 3.6, respectively.

3.A.2. Fe_2O_3 and Sb_2O_4. These two systems were studied as endpoints of the Fe–Sb impregnation series.

Fe_2O_3 was calcined in flowing air for 16 h at 750°C. A surface area of 5.3 m^2/g was measured and the X-ray diffraction data agreed with those for hematite Fe_2O_3 (*23*). XPS showed that there was relatively little C on this sample and no evidence of C build-up during catalyst testing.

Sb_2O_4 was obtained by calcining Sb_2O_3 in air for 2 h at 500°C. This milder treatment was to avoid reducing the surface area. The X-ray diffraction data indicated orthorhombic Sb_2O_4 (*23*) and the surface area determined was 3.2 m^2/g.

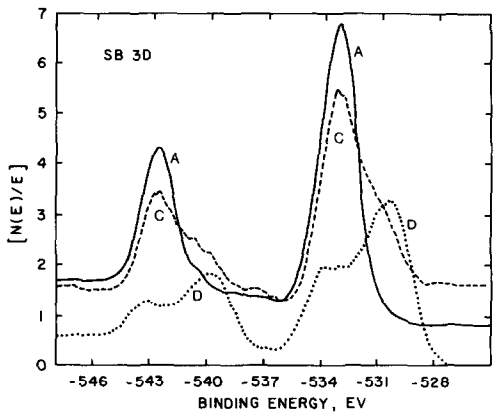

FIG. 2. Effect of gas treatment on $FeSbO_4$. A, $FeSbO_4$ heated in flowing air; C, $FeSbO_4$ heated in flowing helium; D, $FeSbO_4$ + Sb^{3+} heated in flowing helium.

TABLE 5

XPS Atomic Ratios in Al–Sb System

Catalyst	Sb/Al	Sb/Fe	Al/Fe
E = $AlSbO_4$	1.2	—	—
7% Al on E	0.9	—	—
4% Sb on E	1.3	—	—
7% Sb on E	2.4	—	—
7% Fe on E	1.3	17.6	13.5
8% Fe on E	1.0	10.8	11.0
7% Fe on E	1.2	7.0	5.9

3.B. Aluminum–Antimony System

$AlSbO_4$ was prepared by coprecipitation. Calcination at increasing temperatures showed that a single phase and a rutile-type structure could be obtained reproducibly at 1050°C. X-ray diffraction was used to follow the solid-state reaction. All the observed lines the sample match the literature values for rutile $AlSbO_4$ (*23*).

A surface area of 50.7 m^2/g was measured and the XPS analysis of the fresh sample gave 17.1% Sb, 14.8% Al, 57.6% O, and 10.5% graphitic C; resulting in an Sb/Al ratio of 1.2.

Aluminum antimonate was impregnated with extra aluminum, antimony, or iron, to investigate the influence of one metal upon the other. After impregnation, the samples were calcined at 1000°C. No changes were observed in X-ray patterns or surface area measurements.

The XPS atomic ratio of most of the samples are shown in Table 5. Samples 5, 6, and 7, impregnated with approximately the same amount of iron, gave different iron atomic surface concentrations. Samples 5 and 7 were impregnated using the standard procedure; but sample 7 was calcined in oxygen instead of air. Sample 6 was prepared using a solution of iron acetate for impregnation.

$AlSbO_4$, a low activity catalyst (*16*), was used as support and impregnated with different amounts of $FeSbO_4$. Because of the large difference in calcination temperatures required to achieve the $AlSbO_4$ rutile structure, the reverse case of iron antimonate impregnated with aluminum antimonate was not attempted. Heavy loadings of $FeSbO_4$ on $AlSbO_4$ were attained by successive impregnations. After impregnation, the samples were calcined at 750°C.

The amount of $FeSbO_4$ on aluminum antimonate was measured using X-ray diffraction and chemical analysis. An estimate of the extent to which the added iron antimonate could cover the surface of $AlSbO_4$, assuming a slab of uniform thickness was deposited over a semi-infinite flat surface of support, indicates a monolayer of 0.7-Å thickness for a 2% impregnated sample and 6-Å thickness for a 15% $FeSbO_4$ on $AlSbO_4$ surface. The surface compositions are given in Table 6 for fresh and used samples.

The XPS data indicate that the small amount of iron on the surface of the fresh catalysts decreased after use. The amount of Al increased by 2% and there was no significant carbon buildup in the post-run samples. No changes indicative of variations in the cation oxidation states were observed in the shape of the peaks.

3.C. Chromium–Antimony System

This system required extreme conditions to produce a single rutile phase. Samples were prepared by coprecipitation and calcined at 1100°C. There were no powder diffraction data available in the literature

TABLE 6

XPS Results for Iron Antimonate on Aluminum Antimonate: Atomic Concentrations (±10%)

	Sb	Fe	Al	O	C
2% $FeSbO_4$ on $AlSbO_4$					
Fresh	16.5	0.5	6.3	48.1	28.6
Post-run	18.0	Traces	7.8	48.6	25.6
15% $FeSbO_4$ on $AlSbO_4$					
Fresh	19.1	2.8	3.9	53.2	21.0
Post-run	17.9	2.2	5.9	52.1	21.9

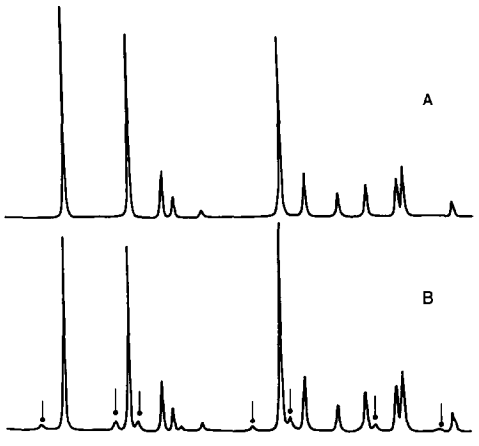

FIG. 3. XRD patterns of $CrSbO_4$ and 7% Cr on $CrSbO_4$. (A) Nonimpregnated and (B) impregnated (—●, extra peak).

for $CrSbO_4$, so a computer pattern giving only line positions was simulated from single-crystal data (*27*). The relative intensities were qualitatively compared with similar rutile compounds. Three batches of the same compound were prepared to ensure that results were reproducible. X-ray measurements of at least three samples of a same batch were taken to average preparation errors.

A surface area of 7.5 m^2/g was determined and the surface composition, XPS, are reported for this catalyst together with the impregnated samples.

Chromium antimonate was impregnated with different amounts of Cr, Sb, and Fe. After impregnation each catalyst was calcined at 1050°C and characterized. There were no changes observed in area measurements. The X-ray diffraction pattern of a sample impregnated with 7% Cr showed the presence of small amounts of Cr_2O_3 along with the rutile $CrSbO_4$ (Fig. 3).

The atomic composition calculated from XPS measurements are given in Table 7. All the fresh samples presented high graphitic-carbon contamination, probably attributable to the tape used in the XPS analysis. The binding energies of the Cr 2*p* peaks coincided with those reported for Cr^{+3}, as in Cr_2O_3 (*28*). Antimony 3*d* peaks showed no particular features.

TABLE 7

XPS Atomic Composition of Chromium Antimonate Catalysts

Catalyst	% Sb	% Cr	% O	% C	% Fe
F = $CrSbO_4$	17.2	5.5	45.5	31.7	—
4% Cr on F	4.7	9.3	42.7	43.3	—
7% Cr on F	5.5	18.1	46.0	30.4	—
7% Sb on F	11.3	1.6	40.5	46.6	—
7% Fe on F	8.7	2.3	48.3	36.1	4.6

3.D. Other Rutile-Related Antimonates

Cobalt antimonate was prepared using the standard coprecipitation method. It was calcined for 16 h at 850°C. X-ray analysis of the sample gave a pattern that matched the trirutile structure of $CoSb_2O_6$ (*23*). The catalyst had a surface area of 1.6 m^2/g. In Table 8 the surface atomic concentration of the elements detected by XPS are shown. The data are for the fresh and used samples and they indicate significant surface enrichment of antimony with an Sb/Co ratio of 3.2 and 2.8, respectively, showing slight variations in the cation surface concentration of the used sample.

A sample of the catalyst was impregnated with 6% Co to investigate its effect on the catalytic performance. After calcining at 800°C, the XPS analysis gave an Sb/Co ratio of 2.2. XPS analysis of the used sample gave a metallic ratio of 2.4, representing a small increase in the surface concentration

TABLE 8

XPS Results for Cobalt Antimony Oxide: Atomic Concentrations (±10%)

	Sb	Co	C	O
$CoSb_2O_6$				
Pre-run	17.5	5.5	33.4	43.6
Post-run	18.8	6.8	31.2	43.2

of both cations. No significant increase in the amount of graphitic carbon was observed.

$RhSbO_4$ was prepared by coprecipitation and calcination at 900°C during 16 h in flowing air. Because there are no powder diffraction data in the literature, the XRD pattern was compared to a computer simulation based on single-crystal data. As in the case of $CrSbO_4$, comparison with similar systems led to the conclusion that the catalyst was single phase, with a rutile structure. A surface area of 9.1 m^2/g was obtained.

The XPS analysis of the fresh sample gave an atomic composition of 11.4% Sb, 2.7% Rh, 54.1% O, and 31.8% graphitic carbon, resulting in a metallic surface ratio of 4.2. The binding energy of the Rh $3d_{(5/2)}$ at 309.9 eV was close to that obtained for compounds where Rh is in +3 state. The used sample had 20.0% Sb, 4.2% Rh, 48.8% O, and 27.0% graphitic carbon. No changes in the shape of antimony and rhodium peaks were observed.

4. DISCUSSION OF RESULTS

Preparation of single phase $MSbO_4$ was essential for the activity measurements performed in these studies. X-ray fluorescence analysis showed absence of impurities in both precursors and final catalysts obtained. With X-ray diffraction, it was determined with a high degree of certainty when a single tetragonal phase has been obtained.

The final temperatures used for all the catalysts studied were lower than those reported by Brandt (*29*), who obtained the same compounds by a physical mixture of the oxides.

Antimony surface enrichment was found by XPS in all catalysts, even the originally biphasic, $FeSbO_4$ + FeO, catalyst. Attempts to bring the *M*/Fe surface ratio close to unity, by impregnation, always resulted in segregation of an iron oxide phase.

On the basis of XPS results, it is clear that the Fe–Sb system is partially reduced under reaction conditions. The presence of Sb^{3+} in the post-run catalyst samples was confirmed by comparison of the helium-treated samples (see Figs. 1 and 2); and Mössbauer studies (*30*) have shown that Fe^{2+} is also present in active catalysts. No other *M*–Sb pair exhibited these features, which may be required for active catalysis.

Regarding whether the Sb-enriched surface layer is $MSbO_4$, MSb_2O_6, or a thin layer of Sb_2O_4 covering the antimonate is not crucial. One of the features common to rutile oxides is the ability to form crystallographic shear (CS) structures (*31*). This not only generates mixed-valence intermediate phases without any profound change in crystal structure, but operates as a means of eliminating point defects by converting them into larger, but less numerous, extended defects which may be clustered and partially ordered. Investigation of such problems is entirely dependent upon electron microscope techniques and are beyond the scope of this work.

We conclude that the dynamics of the surface itself and the flexibility of the rutile structure can explain any reasonable surface structure postulated in the literature.

5. CONCLUSIONS

The synthesis and characterization experiments reported here indicate that it is possible to exchange Fe^{3+} by other M^{3+} cations and to preserve the rutile bulk structure of $FeSbO_4$. However, the coexistence of two such M^{3+} with Sb^{5+} in a single phase is limited to small amounts of one of them. X-ray diffraction showed the segregation of two phases when impregnation went beyond the 7–10% level, depending on the elements involved.

The XPS analysis were conclusive regarding the antimony surface enrichment of most of the catalysts tested and proved that the bulk structure is not a deciding factor defining the change of oxidation state of the cations present in the surface layers. However, the capacity of Sb to be reduced un-

der reaction conditions proved to be critical for the catalytic performance of these oxides. This relationship is established in the next paper in this series (*16*).

REFERENCES

1. Hearne, G. W., and Adams, M. L., U.S. Patent 2,451,485 (1948).
2. Idol, J. D., Jr., U.S. Patent 2,904,580 (1959).
3. Veacth, F., Callahan, J. L., Milberger, E. C., and Foreman, R. W., *in* "Proceedings, 2nd Int. Congr. Catal.," Vol. 2, p. 2647. Technip, Paris, 1960.
4. Veacth, F., Callahan, J. L. and Milberger, E. C., *Chem. Eng. Process.* **5b,** 65 (1960).
5. Adams, C. R., *in* "Proceedings, 3rd Int. Congr. Catal.," Vol. 1, p. 240. Holland, Amsterdam, 1965.
6. Callahan, J. L., and Gertisser, B., U.S. Patent 3,198,750 (1965).
7. Sasaki, T., Nakamura, Y., Moritani, K., Morri, A. and Saito, S., *Catalyst (Japan)* **14,** 191 (1972).
8. Boreskov, G. K., Ven'yaminov, S. A., Dzis'ko, A., Tarasova, D. V., Dindoin, V. M., Sazanova, N. W., Olen'kova, J. P., and Kefeli, L. M., *Kinet. Katal.* **10,** 1109 (1969).
9. Yoshino, T., Saito, S., and Sobukawa, B., Japanese Patent 7,103,438 (1971).
10. Yoshino, T., Saito, S., Ishikara, J., Sasaki, T., and Sofugawa, K., Japanese Patent 7,102,802 (1971).
11. Grasselli, R. K., Heights, G. H., Callahan, J. L. U.S. Patent 3,414,631 (1968). Grasselli, R. K., Heights, G. H., Hardman, H. F., U.S. Patent 3,642,930 (1972).
12. Schuit, G. C. A., and Gates, B. C., *CHEMTECH*, Nov., 693 (1983).
13. Burrington, J. D., Kartisek, C. T., and Grasselli, R. K., *J. Catal.* **87,** 363 (1984).
14. Burrington, J. D., and Grasselli, R. K., *J. Catal.* **59,** 79 (1979).
15. Grasselli, R. K., and Surech, D. D., *J. Catal.* **25,** 273 (1972).
16. Straguzzi, G., Koch, T. and Schuit, G. C. A., *J. Catal.* **104,** in press (1987).
17. Wells, A. F., "Structural Inorganic Chemistry," 4th ed. Oxford Univ. Press (Clarendon), Oxford, 1975.
18. Boreskov, G. K., Ven'yaminov, S. A., Tarasova, D. V., Dindoin, V. M., Sazonova, N. N., Dzis'ko, V. A., and Kefeli, L. M., *Kinet. Katal.* **10,** 1350 (1969).
19. Sala, F., and Trifiro, F., *J. Catal.* **41,** 1 (1976).
20. Sergun'kin, V. N., Pugachev, Y. V., and Popov, I. G., *Zh. Prikl. Khim.* **55,** 1500 (1982).
21. U.S. Patent 3,546,138; Ref. *Zh. Khim.* **13L,** 217 (1971).
22. Zenkovets, G. A., Tarasova, D. V., Nikoro, T. A., and Gadzhreva, F. S., *Kinet. Katal.* **25,** 1243 (1984).
23. International Centre for Diffraction Data, *JCPDS*, (1983).
24. Tricker, M. J., *Inorg. Chem.* **13,** 742 (1974).
25. Burroughs, P., Hamnett, A., and Orchard, A., *J. Chem. Dalton Trans.*, p. 565 (1974).
26. Birchall, T., *J. Chem. Soc. Dalton Trans.*, p. 2003 (1975).
27. Donnay, J. D. H., and Ondik, H. M. (Eds.), "Crystal Data: Determinative Tables," 3rd ed. *JCPDS* **2,** T41–T42 (1973).
28. "Handbook of X-Ray Photoelectron Spectroscopy: Physical Electronics," pp. 72–73.
29. Brandt, K., *Ark. Kemi Mineral. Geol. B* **15,** 1 (1943).
30. Urlich, F. J., Kriegsmann, H., Ohlmann, G., and Scheve, J., *in* "Proceedings, 7th Int. Congr. Catal.," Vol. 2, p. 836. London, 1977.
31. Stone, F. S., *J. Solid State Chem.* **12,** 271 (1975).